05,11

Investigation of Magnetocaloric Effect in a New Perovskite Oxide $La_{0.7-x}Ho_xSr_{0.3}MnO_3$ ($x = 0.2$ and 0.3)

© S. Pal, A. Basu

Institute of Engineering & Management, Management House,
D-1, Sector-V, Saltlake Electronics Complex,
Kolkata-700091, West Bengal, India

E-mail: soumyadipta.pal@gmail.com

Received 11 November, 2022
Revised 13 November, 2022
Accepted 14 November, 2022

The magnetocaloric effect (MCE) of $La_{0.7-x}Ho_xSr_{0.3}MnO_3$ ($x = 0.2$ and 0.3) perovskite oxides has been investigated. A phenomenological model is adopted for simulation of magnetization variation with temperature to investigate magnetocaloric properties such as magnetic entropy change, heat capacity change and relative cooling power. The results indicate the potential of this series of materials to achieve the MCE at temperatures near Curie temperature (T_C). These compounds present as prospective candidates for cooling system in a wide temperature interval in the vicinity of room temperature. The results confirm that the phenomenological model is undoubtedly beneficial for the prediction of the magnetocaloric effect of magnetic materials. Moreover, the effect of holmium (Ho) doping in MCE of $La_{0.7}Sr_{0.3}MnO_3$ has been discussed comparing the results obtained from our calculation for Ho-doped $La_{0.7}Sr_{0.3}MnO_3$ and for non-doped $La_{0.7}Sr_{0.3}MnO_3$ calculated earlier.

Keywords: solid state magnetic refrigeration, phase transition, phenomenological model.

DOI: 10.21883/PSS.2023.02.55413.41

1. Introduction

Refrigeration is one of the most important and extensively used technologies in modern society. Among various methods of refrigeration, magnetic refrigeration (MR) based on the magnetocaloric effect (MCE) with the help of magnetic materials has many advantages over conventional gas refrigeration such as highly efficient cooling, minimal environmental impact, and low cost [1–5]. Incidentally, there is a temperature change in the process of MCE which is associated with the change in entropy of the magnetic material when it is subjected to an applied magnetic field [68]. In last few decades, increasing research interest has been devoted to investigate MR for replacing current process of cooling with hazardous gases which are non-green chemicals such as chloroflurocarbons, hydrochloroflurocarbons, *etc.* at room temperature. This conventional vapor-compression refrigeration techniques cause serious environmental damages like ozone depletion, global warming, *etc.* because of leaks of the working gases. On the other hand, the concept of magnetic cooling is based on the ability of a magnetic substance to change its temperature and entropy under the influence of an adiabatic magnetic field. Eventually, this technology is eco-friendly and leads to significant reduction of power consumption. While refrigeration involves about 15% of the worldwide energy consumption, it has been estimated that MR has the potential to reduce the energy consumption by 20−30 % over the conventional vapor-compression technology [9]. Even at low temperatures, the MR still has drawn attention in gas liquefaction, *e.g.*, hydrogen, helium, *etc.* As a matter of fact, it is important to develop new promising solid-state magnetic materials for magnetic refrigeration operated in a wide temperature range. The essential factor in using MR at room temperature is to find the proper material whose paramagnetic to ferromagnetic transition temperature, *i.e.*, Curie temperature T_C should be near room temperature and which can cause a large entropy variation when it goes through significant magnetization variation with temperature.

Since the discovery of large MCE in $Gd_5(Si_xGe_{1-x})_4$, Gd-based alloys have been primarily investigated for MR devices operating near room temperature [2]. Although the Gd-based materials show a high cooling power near room temperature, high price and susceptibility to oxidation limits their use in commercial cooling devices. Other materials, namely, La-Fe-Si, Mn-Fe-P-As/Si, Fe-Rh, and Heusler alloys also show large MCE at the temperatures of their magnetostructural phase transition near room temperature. However, the large thermal and magnetic hysteresis and narrow working temperature range hinder their use in commercial MR devices [10–12]. Oxide materials such as $R_{1-x}M_xMnO_3$, where $R =$ rare-earth element (La, Pr, Sm, *etc.*), $M =$ alkaline-earth element (Ca, Sr, Ba, *etc.*), are other prospective materials for room temperature MR applications because some of these materials exhibit magnetic phase transitions near room temperature, contain non-toxic and relatively inexpensive elements, and are highly chemically stable [13–18]. $La_{1-x}Sr_xMnO_3$ is one of the most attractive and studied manganite families. Preparation of such material is easy (without the requirement of calcinations process at high temperatures) and cost-effective as well [19].

In the present work, $La_{0.7-x}Ho_xSr_{0.3}MnO_3$ ($x = 0.2$ and 0.3) perovskite oxides (LHSMO) have been chosen in order to investigate their MCE studying the variation of magnetization with temperature at different magnetic fields. It is important to mention that the MCE of LHSMO has not been studied before. We have adopted a phenomenological model [20–29] for the simulation of the temperature dependence of magnetization to predict theoretically the MCE properties of the LHSMO compounds for the first time. This yields further important properties like magnetic entropy change (ΔS), heat capacity change (ΔC), full width at half maximum (δT_{FWHM}), relative cooling power (RCP), *etc.*, as these are the essential parameters for characterizing refrigeration capacity of any compound. The results obtained here convincingly show the effectiveness of such series of materials to obtain MCE. In addition, it may also be concluded that the phenomenological method for the simulation adopted here predicts the MCE of the magnetic materials much precisely. Furthermore, the effect of holmium (Ho) doping in MCE of $La_{0.7}Sr_{0.3}MnO_3$ has been discussed comparing the results obtained from our calculation for Ho-doped $La_{0.7}Sr_{0.3}MnO_3$ and for non-doped $La_{0.7}Sr_{0.3}MnO_3$ calculated by Hamad *et al.* [30].

2. Theoretical formulations

For the theoretical description of magnetocaloric properties, on the basis of phenomenological model proposed by Hamad *et al.* [20–28,30] the dependence of magnetization on temperature T and T_{C} is presented by

$$M(T) = \frac{M_{\mathrm{i}} - M_{\mathrm{f}}}{2} \tanh\left[\alpha(T_{\mathrm{C}} - T)\right] + \beta T + \gamma, \qquad (1)$$

where M_{i} and M_{f} are the initial and final values of magnetization of thermo-magnetization curves with constant magnetic field in the proximity of ferromagnetic to paramagnetic transition, respectively; $\alpha = \frac{2(\beta - S_{\mathrm{C}})}{M_{\mathrm{i}} - M_{\mathrm{f}}}$; $\beta = \left(\frac{dM}{dT}\right)_{T \approx T_{\mathrm{i}}}$ is magnetization sensitivity (dM/dT) at the ferromagnetic state before magnetic transition at $T = T_{\mathrm{i}}$ where initial magnetization M_{i} is developed; $S_{\mathrm{C}} = \left(\frac{dM}{dT}\right)_{T=T_{\mathrm{C}}}$ is magnetization sensitivity at T_{C}; $\gamma = \frac{M_{\mathrm{i}} + M_{\mathrm{f}}}{2} - \beta T_{\mathrm{C}}$.

Now, magnetic entropy change can be calculated by the following equation:

$$\Delta S = \int_0^{H_{\max}} \left(\frac{\partial M}{\partial T}\right)_H dH.$$

After integrating, we obtain

$$\Delta S = \left\{-\alpha \frac{M_{\mathrm{i}} - M_{\mathrm{f}}}{2} \operatorname{sech}^2\left[\alpha(T_{\mathrm{C}} - T)\right] + \beta\right\} H_{\max}. \qquad (2)$$

From Eq. (2), it is clear that the magnetic entropy change increases with increasing magnetization sensitivity dM/dT at T_{C}. The origin of large magnetic entropy change is attributed to high magnetic moment and rapid change of magnetization at T_{C}.

At $T = T_{\mathrm{C}}$,

$$\Delta S_{\max} = H_{\max}\left(-\alpha\left(\frac{M_{\mathrm{i}} - M_{\mathrm{f}}}{2}\right) + \beta\right). \qquad (3)$$

Eq. (3) is important for considering the magnitude of magnetic entropy change to evaluate magnetic cooling efficiency with its full width at half-maximum (δT_{FWHM}).

δT_{FWHM} can be obtained as [29]

$$\delta T_{\mathrm{FWHM}} = \frac{2}{\alpha} \cosh^{-1}\left(\sqrt{\frac{2\alpha(M_{\mathrm{i}} - M_{\mathrm{f}})}{\alpha(M_{\mathrm{i}} - M_{\mathrm{f}}) + 2\beta}}\right). \qquad (4)$$

From Eq. (4), it is apparent that δT_{FWHM} decreases with increasing α, *i.e.*, increasing magnetization sensitivity dM/dT at T_{C} and decreasing the difference $(M_{\mathrm{i}} - M_{\mathrm{f}})$. This equation gives a full width at half-maximum magnetic entropy change contributing for the evaluation of magnetic cooling efficiency as follows. Magnetic cooling is evaluated by considering the magnitude of magnetic entropy change ΔS and its full width at half-maximum, δT_{FWHM}. A product of — $\Delta S_{\max}$ and δT_{FWHM} is called relative cooling power (RCP) based on the magnetic entropy change

$$\mathrm{RCP} = \left(M_{\mathrm{i}} - M_{\mathrm{f}} - \frac{2\beta}{\alpha}\right) H_{\max} \times \cosh^{-1}\left(\sqrt{\frac{2\alpha(M_{\mathrm{i}} - M_{\mathrm{f}})}{\alpha(M_{\mathrm{i}} - M_{\mathrm{f}}) + 2\beta}}\right). \qquad (5)$$

Moreover, the magnetization-related change of the specific heat is given by

$$\Delta C = T \frac{\delta \Delta S}{\delta T}. \qquad (6)$$

Since $dM/dT < 0$, $\Delta S < 0$ and, consequently, the total entropy decreases upon magnetization. Furthermore, $\Delta C < 0$ for $T < T_{\mathrm{C}}$ and $\Delta C > 0$ for $T > T_{\mathrm{C}}$.

ΔC can be derived as [29]

$$\Delta C = -T\alpha^2(M_{\mathrm{i}} - M_{\mathrm{f}}) \operatorname{sech}^2\left[\alpha(T_{\mathrm{C}} - T)\right] \times \tanh\left[\alpha(T_{\mathrm{C}} - T)\right] H_{\max}. \qquad (7)$$

3. Results and discussions

Fig. 1 indicates the variation of magnetization with temperature of $x = 0.2$ and 0.3 compositions of $La_{0.7-x}Ho_xSr_{0.3}MnO_3$. Fig. 1, *a* and *b* represent the thermomagnetization behavior at $x = 0.2$ and 0.3, respectively, with magnetic field $H = 4$, 15, and 50 kOe.

The nature of phase transition is distinctly paramagnetic–ferromagnetic transition with decreasing temperature which is prominent from Fig. 1. In Fig. 1, the symbols represent data taken from [31], while the solid lines indicate the fit

Table 1. Model parameters for $x = 0.2$ and 0.3, with magnetic field $H = 4$, 15, and 50 kOe

Composition x	Magnetic field, kOe	M_i, emu/g	M_f, emu/g	S_C, emu/(g · K)	β, emu/(g · K)	T_C, K
0.2	4	75.702 ± 2.440	12.22 ± 2.290	-1.006 ± 0.052	-0.113 ± 0.020	155.430 ± 1.120
	15	70.452 ± 2.170	24.280 ± 1.880	-0.827 ± 0.043	-0.192 ± 0.017	165.770 ± 1.41
	50	64.389 ± 1.68	40.883 ± 1.33	-0.614 ± 0.040	-0.269 ± 0.010	185.66 ± 2.40
0.3	4	81.736 ± 2.100	0.471 ± 2.32	-0.793 ± 0.022	0.002 ± 0.016	111.40 ± 0.89
	15	98.157 ± 1.290	0.816 ± 0.449	-0.6396 ± 0.0156	0.011 ± 0.005	115.37 ± 1.64
	50	141.860 ± 0.765	1.095 ± 0.647	-0.4783 ± 0.0069	-0.0067 ± 0.0068	103.560 ± 0.945

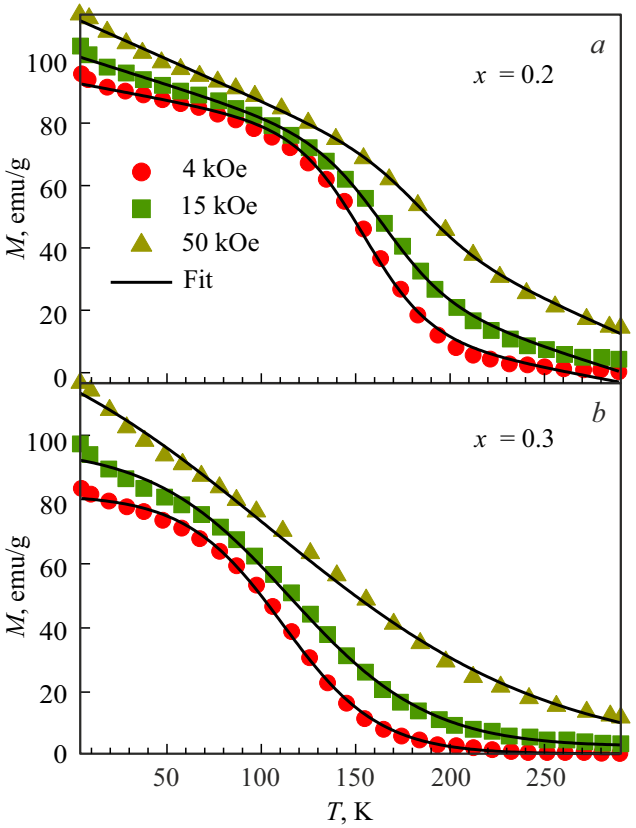

Figure 1. Temperature-dependent magnetization of a — $x = 0.2$ and b — $x = 0.3$, with magnetic field $H = 4$, 15, and 50 kOe. The solid curves are modeled results, and symbols represent experimental data from [31].

using Eq. (1) based on the phenomenological model. The fitting parameters are tabulated in Table 1.

A significant increase in T_C with increasing magnetic field is observed. This indicates an increase in exchange coupling strength between the magnetic dipoles with increasing magnetic field. However, the trend of increasing T_C for $x = 0.3$ at very high field (50 kOe) is reversed. The reason might be the suppression of paramagnetic–ferromagnetic transition due to alignment of magnetic spins along the applied field of very high value.

Subsequently, the temperature variation of modelled magnetic entropy change ΔS of LHSMO at different magnetic fields have been depicted in Fig. 2 using the fitted parameters in Eq. (2). It must be noted that there is onset of large entropy change at T_C which is attributed to high magnetic moment and rapid change of magnetization. This results in an appreciable change in entropy with change in magnetic field also. Furthermore, the position of the peak shifts to higher temperature with the magnetic field, except for very high field (50 kOe) of $x = 0.3$. The reason might be the suppression of paramagnetic-ferromagnetic transition due to alignment of magnetic spins along the large applied field. Interestingly, the magnitude of the entropy change peak ΔS_{max} around T_C increases with increasing magnetic field. Furthermore, the entropy change curves reveal the characteristics of the dipole reorientation. The maximum observed in the ΔS curves are associated with

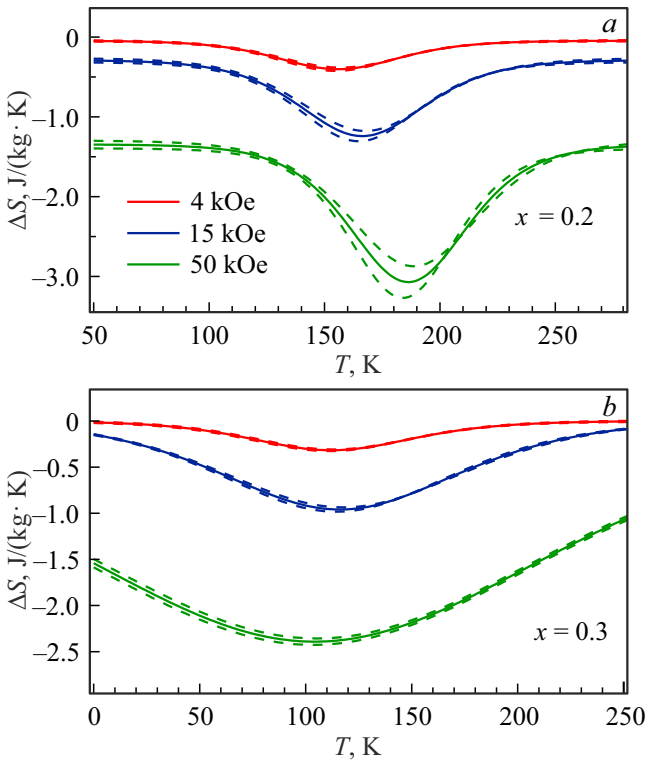

Figure 2. Temperature-dependent magnetic entropy change of a — $x = 0.2$ and b — $x = 0.3$, with magnetic field $H = 4$, 15, and 50 kOe. The dashed line indicates the range of variation of predicted entropy change.

Table 2. The predicted values of maximum magnetic entropy change, full width at half-maximum, RCP, and values of maximum magnetic specific heat change for $x = 0.2$ and 0.3, with magnetic field $H = 4$, 15, and 50 kOe

Composition x	Magnetic field, kOe	ΔS_{max}, J/(kg · K)	δT_{FWHM}, K	RCP, J/kg	ΔC_{max}, J/(kg · K)
0.2	4	-0.402 ± 0.021	69.252 ± 1.705	27.867 ± 0.743	-1.029 ± 0.07 1.390 ± 0.089
	15	-1.241 ± 0.065	81.310 ± 2.830	100.865 ± 1.722	-2.883 ± 0.250 3.843 ± 0.293
	50	-3.070 ± 0.198	120.417 ± 16.152	369.681 ± 38.840	-6.396 ± 1.244 8.137 ± 1.399
0.3	4	-0.317 ± 0.009	90.014 ± 1.013	28.553 ± 1.109	-0.389 ± 0.0013 0.705 ± 0.0038
	15	-0.959 ± 0.023	130.231 ± 2.545	124.944 ± 0.666	-0.740 ± 0.0244 1.696 ± 0.041
	50	2.392 ± 0.035	266.076 ± 2.786	636.320 ± 15.979	-0.495 ± 0.007 2.629 ± 0.009

spins' reorientation that occurs continuously. Thus, the behavior of entropy change patterns suggests how to control the range of temperatures for use in the MCE. Moreover, the shift is confirmed also from the heat capacity study ΔC (Fig. 3) using Eq. (7). It is important to note that the entropy change is not the only parameter which confirms the usefulness of the materials. This is the necessary requirement for the materials which can transport heat at relatively large temperature difference between the cold and the hot sinks in the ideal refrigeration cycle.

Furthermore, the values of the maximum entropy change ΔS_{max}, as well as the full width at half maximum δT_{FWHM}, the relative cooling power RCP, and maximum heat capacity change ΔC_{max} are calculated as shown in Table 2 using Eqs (3)–(5) and (7), respectively.

These are considered to be the important factors for assessing the efficiency of an electronic refrigerant material. It is important to mention that the estimated peak value of ΔS ($|\Delta S_{max}|$) for $x = 0.2$ changes from ~ -0.402 to ~ -3.070 J/(kg · K) and for $x = 0.3$ changes from ~ -0.317 to ~ -2.392 J/(kg · K) due to the magnetic field change from 4 to 50 kOe. The values of ΔS_{max} for these compositions are comparable with other perovskite oxide compounds with large MCE [32–35]. The values of ΔS_{max} obtained confirm the material as prospective candidate for solid state refrigeration in a wide temperature interval above room temperature. Moreover, RCP takes values in range of ~ 27.867 to ~ 369.681 J/kg for $x = 0.2$. For $x = 0.3$, it varies from ~ 28.553 to ~ 636.32 J/kg with the magnetic field change from 4 to 50 kOe. It is important to mention that in application of high magnetic fields an appreciable change in maximum value of specific heat change occurs which recommends LHSMO as one of the promising candidates for solid state refrigeration. It is clear that as applied field increases, the values of $|\delta T_{FWHM}|$, $|\Delta S_{max}|$, RCP, and $|\Delta C_{max}|$ increase. This is attributed to the increasing applied magnetic field, the more induced magnetization, and change during the ferromagnetic-paramagnetic phase transition. The values indicate that LHSMO is significant candidate as

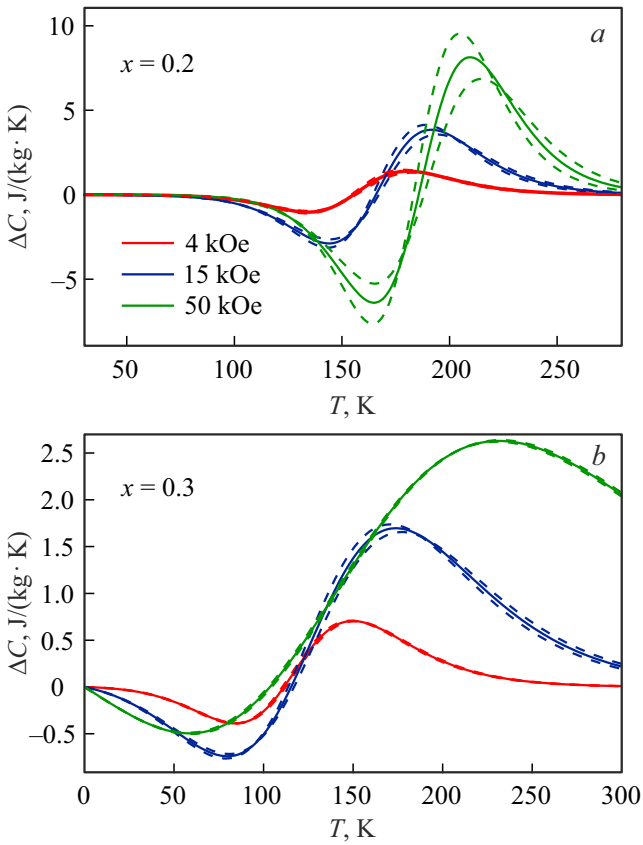

Figure 3. Temperature-dependent heat capacity change of *a* — $x = 0.2$ and *b* — $x = 0.3$, with magnetic field $H = 4$, 15, and 50 kOe. The dashed line indicates the range of variation of predicted entropy change.

magnetocaloric material. It is interesting to observe that the $|\Delta S_{max}|$ and RCP increase with the Ho doping in $La_{0.7}Sr_{0.3}MnO_3$ comparing the values of $|\Delta S_{max}|$ and RCP at 0.4 T for Ho-doped $La_{0.7}Sr_{0.3}MnO_3$ and those values at 0.5 T for non-doped $La_{0.7}Sr_{0.3}MnO_3$ [30].

4. Conclusions

Based on the present phenomenological model, the prediction of magnetocaloric properties of $La_{0.7-x}Ho_xSr_{0.3}MnO_3$ ($x = 0.2$ and 0.3) has been carried out using the extracted thermomagnetization data [31] from magnetization vs temperature curve at different magnetic fields. The magnetization measurements have revealed a ferrmagnetic–paramagnetic transition in a temperature range of 110 to 190 K. Within this temperature span, the MCE of LHSMO is large and tunable. Ho doping in $La_{0.7}Sr_{0.3}MnO_3$ increases the magnetocaloric effect. Thus, this material is excellent candidate among perovskite oxides for working in refrigeration and liquefaction devices in a wide temperature range. Most importantly, phenomenological model helps to calculate magnetocaloric properties of LHSMO with limited processing time and less computational efforts. Thus, this method could be a good alternative to the conventional Arrott plot method [36] for understanding the magnetocaloric effect.

Conflicts of interests

The authors declare that they have no conflict of interest.

References

[1] O. Tegus, E. Brück, K.H.J. Buschow, F.R. De Boer. Nature **415**, *6868*, 150 (2002).
[2] V. Franco, J.S. Blázquez, B. Ingale, A. Conde. Annu. Rev. Mater. Res. **42**, 305 (2012).
[3] M. Balli, B. Roberge, P. Fournier, S. Jandl. Crystals **7**, *2*, 44 (2017).
[4] N.R. Ram, M. Prakash, U. Naresh, N.S. Kumar, T.S. Sarmash, T. Subbarao, R.J. Kumar, G.R. Kumar, K.C.B. Naidu. J. Supercond. Nov. Magn. **31**, *7*, 1971 (2018).
[5] J.H. Belo, A.L. Pires, J.P. Araújo, A.M. Pereira. J. Mater. Res. **34**, *1*, 134 (2019).
[6] A.M. Tishin, Y.I. Spichkin. The Magnetocaloric Effect and Its Applications. Institute of Physics Publishing, Bristol (2003).
[7] K.A. Gschneidner Jr., V.K. Pecharsky, A.O. Tsokol. Rep. Prog. Phys. **68**, *6*, 1479 (2005).
[8] M.H. Phan, S.C. Yu. J. Magn. Magn. Mater. **308**, *2*, 325 (2007).
[9] K.A. Gschneidner Jr., V.K. Pecharsky. Inter J. Refrig. **31**, *6*, 945 (2008).
[10] M. Balli, D. Fruchart, D. Gignoux. J. Phys: Condens. Matter **19**, *23*, 236230 (2007).
[11] M.P. Annaorazov, S.A. Nikitin, A.L. Tyurin, K.A. Asatryan, A.K. Dovletov. J. Appl. Phys. **79**, *3*, 1689 (1996).
[12] X. Zhou, W. Li, H.P. Kunkel, G. Williams. J. Phys: Condens. Matter **16**, *6*, 39 (2004).
[13] M.S. Anwar, S. Kumar, F. Ahmed, N. Arshi, G.W. Kim, B.H. Koo. J. Korean Phys. Soc. **60**, *10*, 1587 (2012).
[14] T. Raoufi, M.H. Ehsani, S.D. Khoshnoud. Ceram. Int. **43**, 5204 (2017).
[15] M. Zarifi, P. Kameli, M.H. Ehsani, H. Ahmadvand, H. Salamati. J. Alloys. Compd. **718**, 443 (2017).
[16] M. Kumaresavanji, C.T. Sousa, A. Pires, A.M. Pereira, A.M.L. Lopes, J.P. Araujo. Appl. Phys. Lett. **105**, *8*, 083110 (2014).
[17] M.H. Ehsani, P. Kameli, M.E. Ghazi, F.S. Razavi, M. Taheri. J. Appl. Phys **114**, **22**, 223907 (2013).
[18] A. Rostamnejadi, M. Venkatesan, P. Kameli, H. Salamati, J.M.D. Coey. J. Appl. Phys. **116**, *4*, 043913 (2014).
[19] D.R. Sahu, B.K. Roul, P. Pramanik, J.-L. Huang. Physica B **369**, *1–4*, 209 (2005).
[20] M.A. Hamad. Phase Trans. **85**, *1–2*, 106 (2012).
[21] M.A. Hamad. J. Adv. Ceram. **1**, *4*, 290 (2012).
[22] M.A. Hamad. J. Supercond. Nov. Magn. **26**, *3*, 669 (2013).
[23] M.A. Hamad. Phase Trans. **87**, *5*, 460 (2014).
[24] M.A. Hamad. J. Supercond. Nov. Magn. **27**, *11*, 2569 (2014).
[25] M.A. Hamad. J. Supercond. Nov. Magn. **28**, *7*, 2223 (2015).
[26] M.A. Hamad. J. Supercond. Nov. Magn. **29**, *11*, 2867 (2016).
[27] A.H. El-Sayed, M.A. Hamad. J. Supercond. Nov. Magn. **31**, *6*, 1895 (2018).
[28] A.H. El-Sayed, M.A. Hamad. J. Supercond. Nov. Magn. **31**, *10*, 3357 (2018).
[29] S. Pal, S. Datta. J. Supercond. Nov. Magn. **34**, *11*, 2905 (2021).
[30] M.A. Hamad. J. Adv. Ceram. **2**, *3*, 213 (2013).
[31] P. Raychaudhuri, T.K. Nath, P. Sinha, C. Mitra, A.K. Nigam, S.K. Dhar, R. Pinto. J. Phys.: Condens. Matter **9**, *49*, 10919 (1997).
[32] N. Kallel, S. Kallel, A. Hagaza, M. Oumezzine. Physica B **404**, *2*, 285 (2009).
[33] A. Rostamnejadi, M. Venkatesan, P. Kameli, H. Salamati, J.M.D. Coey. J. Magn. Magn. Mater. **323**, *16*, 2214 (2011).
[34] A. Rostamnejadi, M. Venkatesan, J. Alaria, M. Boese, P. Kameli, H. Salamati, J.M.D. Coey. J. Appl. Phys. **110**, *4*, 043905 (2011).
[35] S. Vadnala, S. Asthana. J. Magn. Magn. Mater. **446**, 68 (2018).
[36] A. Arrott. Phys. Rev. **108**, *6*, 1394 (1957).